

Late Glacial and Holocene multi-proxy environmental reconstruction from Lake Hakluyvatnet, Amsterdamøya Island, Svalbard (79.5°N)

Marthe Gjerde^{1,2}, Jostein Bakke¹, William D'Andrea³, Nicholas S. Balascio^{3,4}, Raymond S. Bradley^{1,5}, Kristian Vasskog¹, Sædis Ólafsdóttir¹, Torgeir O. Røthe¹, Bianca B. Perren⁶, Anne Holmes^{2,7}

¹ Department of Earth Science and Bjerknes Centre for Climate Research, University of Bergen, Allégaten 41, 5007 Bergen, Norway

² The University Centre in Svalbard, 9171 Longyearbyen, Norway

³ Lamont-Doherty Earth Observatory of Columbia University, Palisades, NY, USA

⁴ Department of Geology, College of William & Mary, Williamsburg, VA, USA

⁵ Department of Geosciences, University of Massachusetts, Amherst, MA 01003, USA

⁶ British Antarctic Survey, High Cross, Madingley Road, Cambridge, UK CB3 0ET

⁷ Department of Earth Sciences, University of Gothenburg, SE-405 30 Gothenburg, Sweden

Corresponding author: Marthe Gjerde, Department of Earth Science, University of Bergen, Allégaten 41, NO-5007 Bergen, Norway. E-mail: Marthe.gjerde@uib.no. Phone: +47 55 58 81 10.

Keywords: Lake sediments, Runoff, Svalbard, Holocene, Neoglacial, Multi-proxy analyses

ABSTRACT

Robust records of past climatic changes are sparse and poorly resolved in the Arctic due to low organic production that restricts the use of radiocarbon dating and challenging logistics that make data collection difficult. Here, we present a new lake record from lake Hakluytvatnet at Amsterdamøya island (79.5°N), the northwesternmost island on Svalbard. Multi-proxy analyses of lake sediments in combination with geomorphological mapping reveal large environmental shifts that have taken place at Amsterdamøya since the Late Glacial. A robust chronology has been established for the lake sediment core through 28 AMS radiocarbon (^{14}C) ages, and this gives an exceptionally well-constrained age control for a lake at this latitude. The sedimentary archive recorded the last ~13,000 years of climate change, and is the first lake record going back to the Late Glacial at this site. Our findings indicate that a local glacier was present during the Younger Dryas (YD), and we estimate YD equilibrium-line altitude (ELA) lowering. Further, the Holocene was a period with large changes in the Hakluytvatnet catchment, and the onset of the Neoglacial (ca. 5 ka) marks the start of modern-day conditions in the catchment. The Neoglacial is characterized by fluctuations in the minerogenic input to the lake as well as internal productivity, and we suggest that these fluctuations are driven by atmospherically forced precipitation changes as well as sea ice extent modulating the amount of moisture that can reach Hakluytvatnet.

1. INTRODUCTION

Palaeoclimatic reconstructions offer the possibility to extend earth system observations beyond the instrumental time period. Such reconstructions are especially important in the Arctic because the rate of on-going change is unprecedented within Common Era observations. However, our knowledge of the natural climate variability in the Arctic is limited due to the scarcity of data and the relatively short period of observation. Future anthropogenic climate changes will be superimposed on these natural variations, which might result in fundamental changes to internal climate feedback mechanisms, influencing the timing and amplitude of future climate. This leads to a critical emerging question in the scientific community: how will the effects of global warming be manifested in the Arctic? To make meaningful climate projections at the regional scale and to evaluate model simulations of future climate, we need a longer perspective than the short instrumental period provides. Annual precipitation in the Arctic is projected to increase by 20% by the end of the twenty-first century (ACIA, 2004), among the highest globally, and this is a consistent feature among state-of-the-art global climate models (Kattsov et al., 2007). The anticipated climate changes, and especially those related to hydrology, will have a large impact on sources and sinks of greenhouse gases related to the Arctic tundra (Jørgensen et al., 2015), on local societies in the Arctic, and will likely impact lower latitudes through climatic teleconnections (Førland et al., 2009). However, to better anticipate future changes in the Arctic, a significant improvement in our documentation and understanding of the longer-term natural climate variability in this region is required. Due primarily to logistical constraints, the region north of 70°N is heavily under-sampled with respect to Holocene paleoclimate reconstructions.

Svalbard, a high-Arctic Norwegian archipelago (74-81°N, 10-35°E), is situated in a climatically sensitive site in the northern North Atlantic and is well-positioned to record past changes in atmospheric and oceanic circulation patterns of the North Atlantic Arctic. Lake

sediments are excellent archives for recording regional climate change, because lakes trap detrital and organic material from the catchment, as well as organic material produced within the lake. The type of material entering the lake depends on the catchment area surrounding the lake basin (Rubensdotter and Rosqvist, 2009), and this in turn depends on a number of geological, geomorphological and climatic factors. Sedimentary fingerprinting of the various sources contributing to lake sedimentation and their past variations allows for detailed palaeoenvironmental reconstructions.

Here we present new palaeoclimatic data from one of the northernmost lakes in Europe, on Amsterdamøya island, NW Svalbard. We demonstrate that the potential for producing robust chronologies exists even in these remote polar regions, and that by careful selection of sites high-resolution palaeoclimatic reconstruction can be achieved. Here we present: 1) a high precision radiocarbon dated sedimentary lake sequence; 2) reconstructed glacier activity and detrital sedimentation processes from the Late Glacial until the present; and 3) a multi-proxy reconstruction of Neoglacial climate fluctuations at Amsterdamøya based on the runoff and productivity signal recorded in the lake sediments.

2. SETTING

The island of Amsterdamøya (‘øya’=island) (N79°46’, E10°45’) is located at the northwesternmost corner of Svalbard in the North Atlantic Ocean, where the distance from Amsterdamøya to the shelf break is only 8 km. The West Spitsbergen Current (‘WSC’) (Aagaard et al., 1987) is the northernmost limb of the Norwegian Atlantic Current (‘NwAC’), bringing warmer Atlantic waters as an extension of the North Atlantic Current (‘NAC’) to the NW coast of Svalbard (Fig. 1A). Due to this northward transport of warm water and its impact on air masses, the western side of the Svalbard archipelago is dominated by warmer

temperatures, more precipitation and less sea ice than the east coast. On the coast of western Svalbard (Ny-Ålesund and Isfjord Radio) (Fig. 1A) summer temperature (June, July, August) (1961-1990) averages 4°C, and averages range from -12 to -15 °C during the winter months (January, February, March; JFM). Winter (JFM) precipitation on Svalbard ranges from 190-440 mm/year (Førland et al., 2010). The alternating westerlies and the polar-front jet stream modulate the present climate on Svalbard and are influenced by the North Atlantic Oscillation (NAO) and the Arctic Oscillation (AO). During positive AO (AO+) winters, cyclones reach the Barents Sea region thereby bringing more snow to Svalbard; conversely, a negative AO (AO-) leads to a tendency toward NE-E winds, cold temperatures, and lower winter precipitation (e.g Luks et al., 2011).

A metamorphosed basement comprised of migmatites, banded gneisses rich in biotite and late-tectonic granites of Caledonian age form the bedrock in the area. Small outcrops of amphibolite are present on the north side of the catchment, as well as small appearances of marble layers on the north and south side of the catchment area (Hjelle and Ohta, 1974; Ohta et al., 2007). Amsterdamøya island is characterized by gently sloping plateaus >300 m a.s.l. covered by autochthonous block fields. Steep cliffs towards the sea frame the plateaus (Hjelle and Ohta, 1974).

Surface exposure ages on glacial erratics from Amsterdamøya and the neighbouring Danskøya islands (Fig. 1B) indicate that the summits in the area have remained ice-free since >80 ka BP, although the lower grounds remained glaciated until 18-15,000 years ago (Landvik et al., 2003). These more recent ages are further supported by surface exposure ages from Hormes et al. (2013), indicating that the NW sector of Svalbard became deglaciated between 13,600 and 11,700 years ago after a local ice dome covering the NW Svalbard disintegrated. The marine limit (ML) at Amsterdamøya is not constrained, but is probably close to present day sea level (Boulton and Rhodes, 1974; Salvigsen, 1979; Landvik et al.,

1998). There has been little postglacial emergence in the NW part of Svalbard, and neither Amsterdamøya nor Danskøya display clear geomorphological evidence of uplift in relation to sea level since the ice cover disappeared (Boulton and Rhodes, 1974; Salvigsen, 1977; Landvik et al., 1998).

2.1 Lake, catchment, and geomorphological setting

Our study site, lake Hakluytvatnet (79°46'24"N, 10°44'21"E) (12 m a.s.l.) is a small lake with a surface area of ~0.1 km² (Fig. 1A). The catchment area (~2.2 km²) displays steep cliffs incised by two cirque valleys surrounding the flat valley floor. The northwest-facing beach sequence framing the lake forms a terrace towards the sea (Fig. 1C), and consists of well-rounded gravel-and-boulder type beach sediments. Maximum water depth of Hakluytvatnet ('vatnet'=lake) is ~5 m, and the lake is surrounded by 'northern arctic-tundra zone'-type vegetation (Birks et al., 2004). The lake has a pH of 5.9, conductivity values are low and filamentous algae are frequent in the lake and in the lake outflow with extensive submerged moss growth even at 5 m water depth (Birks et al., 2004). Hydrolab field measurements in September 2014 revealed that the lake water had a temperature of 4°C, and that the water was well-mixed by wind and showed no stratification. The geometry of the lake basin is shallow, and it dips gently towards the deepest part where maximum sediment thickness is ~2.5 m (Fig. 1D). At present, there are no glaciers in the catchment; however, two perennial snow patches are present on the plateau in the southern part of the catchment serving as the main source area for the river feeding Hakluytvatnet (Fig. 1C).

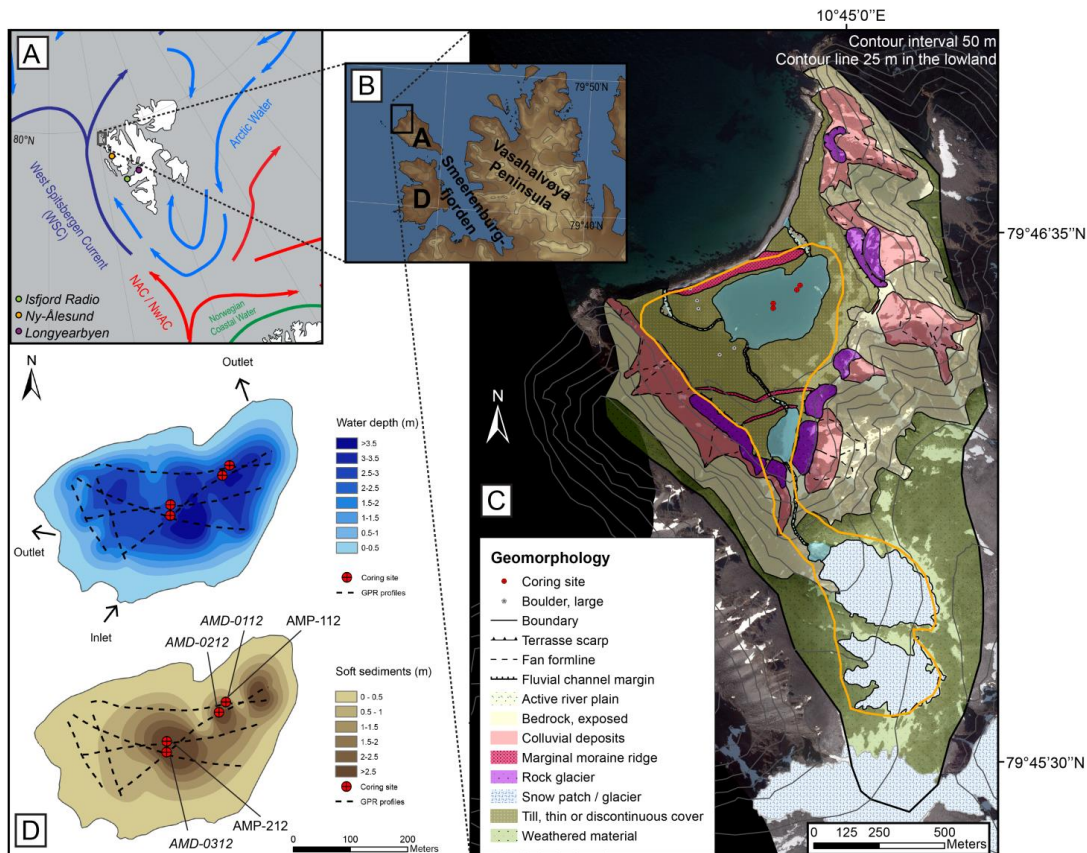


Figure 1: A) Svalbard and surrounding surface currents; B) NW corner of Svalbard (topographic) with place names: A=Amsterdamøya, D=Danskøya; C) Geomorphological map of the study site and catchment area. Orange line denotes inferred former glacier extent (cf. section 4.6; D) Bathymetrical map (top) and soft-sediment thickness (below) with coring sites and GPR profiles. Base maps: Norwegian Polar Institute. Ocean currents data: Institute of Marine Research, Norway.

3. METHODS

The environmental reconstruction in this study is based upon a combination of geomorphological mapping (orthophoto: Norwegian Polar Institute, series S2011_25160), field ground-truthing, lake coring, and multi-proxy laboratory analyses. A firm chronology has been established for the lake sediments from AMS radiocarbon dating.

3.1 Lake coring and laboratory analyses

Prior to lake coring in late summer 2012, Hakluyvatnet was surveyed using a Ground Penetrating Radar (GPR) in order to map the bathymetry and the sediment distribution before determining suitable coring sites. GPR profiles were collected using a RAMAC GPR from Malå with a 50 MHz RTA antenna (Fig. 1D). In total, 5 cores were extracted; 2 piston cores (AMP-112; 170 cm; and AMP-212; 247.5 cm) and 3 gravity cores (AMD-0112; 142 cm; AMD-0212; 42 cm; and AMD-0312; 56 cm) (see Fig. 1D for coring locations). AMD-0212 (core data presented in Balascio et al., this issue) was sampled every 0.5 cm of the top 10 cm while in the field to obtain samples for ^{210}Pb dating. During a second field excursion (late summer 2014), measurements of the lake water properties (using a Hydrolab multiparameter water quality instrument) were made, and more detailed mapping of the catchment area was conducted, including extensive GPR surveying of the beach sequence damming the lake.

The sediment cores AMP-112 and AMP-212 were split lengthwise in the lab and one half of each core were stored for reference. During splitting, both core sections of AMP-212 were disturbed, and this core was therefore not subject to further analyses. Core AMP-112 was carefully cleaned and photographed before lithofacies and sedimentological structures were described based on visual inspection.

For core AMP-112 we measured weight loss-on-ignition (LOI), dry bulk density (DBD) and water content (WC) (Dean, 1974; Heiri et al., 2001) every 0.5 cm ($n = 339$) using a syringe for fixed volume extraction (1 cm^3). This method was applied for the more minerogenic part of the core (below 105 cm depth), whereas for the uppermost 105 cm, where abundant aquatic mosses made it more difficult to apply the syringe (see section 4.2), samples were extracted using a scalpel. The DBD (volume-dependent) measurements for the upper part were therefore considered less accurate. Down-core variations in surface magnetic susceptibility

(MS) were measured on the split cores at 0.2 cm resolution using a Bartington MS2E point sensor.

Geochemical data and radiographic images of AMP-112 were obtained using an ITRAX X-ray fluorescence (XRF) scanner (Croudace et al., 2006) at EARTHLAB, University of Bergen. A molybdenum (Mo) X-ray tube was used for radiographic measurements, whereas XRF analyses were performed applying a chromium (Cr) tube, with a down-core resolution of 500 μm . XRF power settings of 30kV and 40 mA were used with a 10 s counting time. Due to the differences in sediment composition and organic content in the different core sections, we applied normalization using the conservative redox-insensitive element aluminium (Al) (Thomson et al., 2006; Löwemark et al., 2011) as a supplement to the single elemental count rates.

AMP-112 was sampled every cm down-core (from 3-170 cm depth; $n = 167$) for grain size distribution (GSD) analysis (averaged over 5 runs of each sample), using the Mastersizer 3000 from Malvern Instruments Ltd. connected to the Hydroseries wet dispersion unit allowing for laser diffraction measurement of particle sizes (Ryzak and Bieganowski, 2011). Particle absorption index was set to 0.01; particle refractive index to 1.8, and the pump speed was 2400 rpm. 60% ultra-sonication was applied for 60 s before analysis for all samples, and each measurement was set to 25 s counting time (Sperazza et al., 2004; Ryzak and Bieganowski, 2011).

Six samples were chosen for diatom analysis from 97, 108, 130, 150, 158, and 160.5 cm depth in the core to investigate the possible presence of a marine transgressive unit. Diatoms were isolated from the sediments using standard oxidative techniques modified from Renberg (1990) and mounted on glass coverslips using Naphrax mounting medium. At least 300 diatom samples were identified from each slide at 1000x under oil immersion and identified

using predominantly arctic diatom floras (e.g. Antoniadou et al., 2008). Constrained cluster analysis (CONISS, broken stick model) performed in the open-source statistical software 'R' (R Development Core Team, 2012) delineated the significant stratigraphic zones.

3.2 Radiocarbon dating, palaeomagnetic secular variations and age-depth relationship

The surface top 10 cm including the sediment-water interface in core AMD-0212 were extracted in the field for ^{210}Pb dating. Although the resulting analyses were unsuccessful in establishing a lead profile for accurate chronological constraint, they revealed lead activity in the top demonstrating that the sediments on top of AMD-0212 are modern. For radiocarbon dating, a total of 31 plant macrofossil fragment samples were extracted from cores AMD-0212/AMP-112 (3 of the samples did not contain enough carbon to be dated; see Table 1). An age-depth relationship was established using the Bayesian framework calibration software code 'Bacon' (v. 2.2; Blaauw and Christen, 2011), applied into 'R' (v. 3.2.2). Radiocarbon ages are reported in calibrated radiocarbon years before present ('cal yr BP'; BP=1950) according to IntCal13 (Reimer et al., 2013).

We then attempted to further constrain this radiocarbon age-depth relationship by applying a palaeomagnetic method known as palaeomagnetic secular variations (PSV) (e.g. Merrill et al., 1996). As sediment archives can contain continuous information on the fine-scale variations of the geomagnetic field, reconstruction of PSV may serve as an independent stratigraphic tool in various sediment environments (e.g. Stoner and St-Onge, 2007). A PSV-reconstruction was therefore carried out on core AMP-112 among other sediment archives from Svalbard (Ólafsdóttir et al., this issue). This allowed for PSV-based synchronization between AMP-112 and another ^{14}C -dated lacustrine sediment core 'HAP0212' from Lake Hajeren, a glacier-fed lake ca. 60 km south of Amsterdamøya (van der Bilt et al., 2015). Based on the PSV-

correlation, a total of 43 radiocarbon dates from both cores were combined to a single composite age-model where each radiocarbon date was PSV-correlated within the 2σ radiocarbon calibration uncertainty range (with some exceptions, c.f. section 5.1/Ólafsdóttir et al., this issue), resulting in a mutual depth scale and age-depth relationship for further proxy comparison. Additional details on the PSV-synchronization and construction of the composite age model are discussed in Ólafsdóttir et al. (this issue).

Table 1: Radiocarbon ages AMD-0212 and AMP-112. Samples in italics: Could not be dated. $\delta^{13}\text{C}$ values: graphitisation process introduces significant isotopic fractionation. *: Estimate of carbon content (50%) from the sample mass. Calibrated applying IntCal13 curve.

Core	Lab.no.	Depth (cm)	Material	^{14}C age	Error +/- 1 sigma	+/- 2 sigma (cal yr BP)	$\delta^{13}\text{C}$ ‰	mg C
AMD-0212	D-AMS 006994	11-12	Plant remains	335	23	312-468	-28.1	1.05*
AMD-0212	D-AMS 006995	15.5-16.5	Plant remains	590	22	541-646	-20.7	1.10*
AMD-0212	D-AMS 006996	20-21	Plant remains	1006	20	835-963	-21.9	1.35*
AMD-0212	D-AMS 006997	31-32	Plant remains	1778	24	1617-1808	-21.1	1.00*
AMP-112	Ua-48155	4-5	Plant remains	1481	30	1307-1411	-19.7	1.11
AMP-112	Ua-48156	6-7	Plant remains	1638	31	1416-1612	-21	0.66
<i>AMP-112</i>	<i>Ua-48156</i>	<i>6-7</i>	<i>Chironomid head capsules</i>	-	-	-	-	-
AMP-112	Ua-48157	11.5-12.5	Plant remains	1432	30	1295-1376	-19.1	0.74
AMP-112	Ua-48158	17.5-18.5	Plant remains	1860	30	1720-1869	-21.2	1.39
AMP-112	Ua-48159	22.5-23.5	Plant remains	1895	30	1737-1897	-22.1	1.29
AMP-112	Ua-48160	25.5-26.5	Plant remains	1925	31	1816-1947	-20.8	1.09
AMP-112	Ua-48161	31.5-32.5	Plant remains	2025	31	1896-2099	-21.3	1.07
AMP-112	Ua-48162	35-36	Plant remains	2100	30	1997-2144	-20.4	1.17
<i>AMP-112</i>	<i>ETH-49504</i>	<i>38-39</i>	<i>Chironomid head capsules</i>	-	-	-	-	-
AMP-112	Ua-48163	45-46	Plant remains	2564	30	2506-2754	-21.3	1.09
AMP-112	Ua-48164	50.5-51.5	Plant remains	2589	30	2545-2767	-19.2	1.07
AMP-112	Ua-48165	60.5-61.5	Plant remains	2859	30	2879-3064	-20.5	1.06
AMP-112	Ua-48166	73-74	Plant remains	3458	30	3641-3828	-21.6	1.18
AMP-112	Ua-48167	77.5-78.5	Plant remains	3433	30	3608-3826	-21.1	1.33
AMP-112	Ua-48168	85.5-86.5	Plant remains	3783	34	4006-4284	-21.7	1.07
AMP-112	Ua-48169	98.5-99.5	Plant remains	4293	33	4826-4959	-23.6	1.10
AMP-112	Poz-70631	104.5-105.5	Plant remains	4575	35	5055-5446	-17.4	1.10
AMP-112	ETH-49505	110-111	Plant remains	7107	56	7827-8023	-46.3	0.13
AMP-112	Ua-48170	121-122	Plant remains	7823	51	8455-8770	-25.1	0.006
AMP-112	Ua-48171	132-133	Plant remains	8236	50	9032-9399	-25	0.25
AMP-112	Ua-48172	141-142	Plant remains	7934	60	8610-8988	-25	0.05
AMP-112	ETH-49506	144-145	Plant remains	8718	52	9550-9887	-38.2	0.28
AMP-112	Ua-48173	156-157	Plant remains	10968	61	12719-12991	-25.9	1.44
<i>AMP-112</i>	<i>ETH-49507</i>	<i>158-159</i>	<i>Plant remains</i>	-	-	-	-	-
AMP-112	ETH-49508	162-163	Plant remains	10835	86	12614-12943	-63.5	0.11
AMP-112	ETH-49509	167-168	Plant remains	11008	55	12735-13014	-24.0	0.16

3.3 Multivariate analysis

Principal Component Analysis (PCA) was applied in order to explore the multi-proxy dataset from Hakluyvatnet, including LOI, variations in the 90th percentile of the grain size distribution (GSD90) and 10 geochemical elements (Al, K, Ca, Rb, Ti, Fe, Si, Mg, Mn, Sr) obtained from the ITRAX XRF scan. Regression analyses revealed a logarithmic relationship between many of the variables, which warranted a log transformation of all data before running the PCA, as the analysis assumes linearity between the included variables (e.g. Bakke et al., 2013). All of the data were then standardized before running the PCA in Canoco for Windows (v. 4.5; Lepš and Šmilauer, 2003).

RESULTS

4.1 Geomorphic mapping

An exposed seaward section of the beach sequence damming Hakluyvatnet has previously been studied by Landvik et al. (2003) and was interpreted as a succession of marine and glacial proximal sediments underlying glaciolacustrine sediments, capped by subglacial till containing large angular boulders. The section was dated by Landvik et al. (2003), with optically stimulated luminescence (OSL) ages clustering around 50 ka BP in the sub-till section, and correlated with the Kapp Ekholm interstadial (Mangerud et al., 1998). Here we interpret the topmost part of the ridge (16 m a.s.l.) as a marginal moraine (Fig. 1C). There are two outlets from Hakluyvatnet cutting down and through the ridge; in the east and in the west. GPR measurements across the ridge showed that the ridge is composed only of unconsolidated sediments, meaning that there is no bedrock threshold within the landform damming Hakluyvatnet.

Ridge-shaped lobate landforms consisting of large angular blocks with only sparse vegetation cover are present in large parts of the catchment area. These follow the mountain sides as a continuation of talus (Fig. 1C) and terminate in the sea on the north side of the catchment. These landforms are interpreted as rock glaciers (e.g. Swett et al., 1980), a feature frequently observed in polar regions like Svalbard. The rock glaciers are ice-cored and appear to be talus-derived (Shakesby et al., 1987). Two sets of smaller ridges in the southern cirque valley are interpreted as two generations of recessional moraines (Fig. 1C). The remainder of the valley floor is draped by a thin or discontinuous cover of till.

4.2 Lake core lithostratigraphy

The AMP-112 core was divided into 5 main stratigraphic units: A, B, C, D and E, based on visual logging (Fig. 2). A grain-size distribution (GSD) surface plot (Fig. 3) shows the main grain-size mode changing accordingly between the lithostratigraphic units. A cumulative plot of the GSD (Fig. 3) highlights the silt-sized grains constituting the background sediment in the AMP-112 record; where on average ~80% of the sediment is 63 μm or smaller.

Unit A (170-159 cm) consists of a grey to olive brown matrix-rich diamict. The unit is massive, over-consolidated, and poorly sorted. The organic content (LOI) is low (~5% for most of the unit), water content is close to zero (~4 %) whereas the density (DBD) values are relatively high (~1.1 g/cm³). The X-ray image (Fig. 2) shows the dense character of the unit, reflected by the dark colouring. Geochemical elements reflecting minerogenic content (e.g. Ti, Al, Ca, K) hold their highest values throughout the core in unit A. Unit A is the only unit where MS shows high amplitude fluctuations from 6 up to 22 (Si 10⁻⁵) (MS results not shown in Fig. 2 due to near-zero values throughout the rest of the core). Grain sizes range from clay to gravel, with clasts >2.5 cm and a matrix dominated by sand (~50%) and silt (~48%) (Fig.

3). Sub-rounded to sub-angular clasts $>2500\ \mu\text{m}$ are scattered throughout the unit, and these large clasts were removed before GSD analysis. Small amounts of terrestrial macrofossils were present and 2 samples from unit A were sent for radiocarbon dating (Table 1). From 159.3-159 cm depth, a pale yellow to grey horizon consisting mainly of clay, silt and very fine sand is visually prominent (Fig. 2). This horizon is considered to represent an ‘event’ layer, i.e. a layer of instantaneous deposition. The transition between units A to B is sharp.

Unit B (159-155 cm) consists of olive/dark brown laminated silty sediments, with mosses intertwined. Laminations range from $<1\ \text{mm}$ up to 2 mm. The transitions below and above are sharp. The layering of this 4-cm thick section is chaotic, and it contains a mix of grain sizes from clay and silt ($\sim 72\%$) to sand ($\sim 24\%$). LOI increases from the low values in Unit A to an average of $\sim 12\%$, whereas DBD decreases to average $\sim 0.7\ \text{g/cm}^3$. Because the geochemistry (sulphur peak in Fig. 2) indicated that that Unit B potentially represented a marine-brackish transition, we performed diatom analyses in order to investigate the potential for a marine impact on lake sedimentation. Diatom results (cf. Section 4.3 below) revealed that Hakluytvatnet holds a terrestrial and (freshwater) aquatic signal throughout the whole record.

Unit C (155-109 cm) consists of olive brown to very dark greyish brown laminated silty gyttja. Laminations are finest in the lowermost part (155-142.5 cm), which is also detected in X-ray imagery (Fig. 2). LOI ranges from $\sim 13\%$ to $\sim 35\%$, with a mean of $\sim 26\%$ and a trend of increasing organic content upwards where the highest values are found between 142 and 119.5 cm. DBD values range from 0.15 to $0.60\ \text{g/cm}^3$, with a mean value of $\sim 0.22\ \text{g/cm}^3$. Grain sizes vary in range from clay to coarse sand (Fig. 3), with most of the sediment being silt-sized, on average $\sim 77\%$. A small, minerogenic light yellowish brown horizon from 142.5-142 cm with sharp transitions above and below is characterised by a drop in organic content and a peak in DBD, which is also reflected in the X-radiographic image. Clay and very fine

silt also peaks at this depth, as well as increased Ti count rates indicating more detrital input. We consider that this thin layer might represent an instantaneous depositional event; however, it is not omitted from age-depth modelling. At 120.5-119.5 cm depth a light-coloured minerogenic horizon can be seen, which is characterized by greater clay and silt content (~84%) than the section below. Density increases are reflected in both DBD and X-ray imagery, and organic content drops to <15%. As with the above-mentioned light-coloured horizon at 142.5-142 cm, we acknowledge that this layer might represent an event, however; the gradual transitions to this layer indicates that it might represent normal sedimentation, and it is therefore not omitted from the age-depth modelling.

Unit D (109-105 cm) consists of massive, olive brown gyttja silt with an irregular transition to Unit C below. LOI averages ~16% and DBD averages 0.34 g/cm³. The higher density in this unit compared to unit C below can also be seen in the X-radiographic image. The geochemical detrital parameters increase (Ti, Ti/Al) as well as Si/Ti indicating a potential increase in lake productivity (Fig. 2). Small amounts of macrofossils are present. GSD (Fig. 3) shows that this section contains less clay (averaged ~2.9%) than the sections above and below, and that it consists mainly of silt (~71%) and sand (~26%), with most of it belonging in the range of medium silt to very fine sand.

Unit E (105-0 cm) consists of organic olive brown and very dark brown gyttja, where aquatic mosses are abundant throughout the unit. Weak laminations displaying different colouring and minerogenic content than the dominant dark brown organic-rich facies are visible, and are also reflected in the varying density seen in the X-ray image (Fig. 2). Water content is high (>96% at certain depths) throughout the unit, and some of the geochemical minerogenic indicators reflect this by yielding lower count rates in this section (Ti count rates in Fig. 2) (Tjallingii et al., 2007). LOI is on average ~29%, ranging from ~16 to ~43%. Sediments are predominantly silt-sized, with the highest averaged silt values in the core

~80%, ranging from ~65-86%. Sand content is on average ~17%; ranging from ~11-33% with most of it ranging from very fine to fine sand. From 66-62 cm depth and from 7-3 cm depth a relative increase in grain size is observed (Fig. 3).

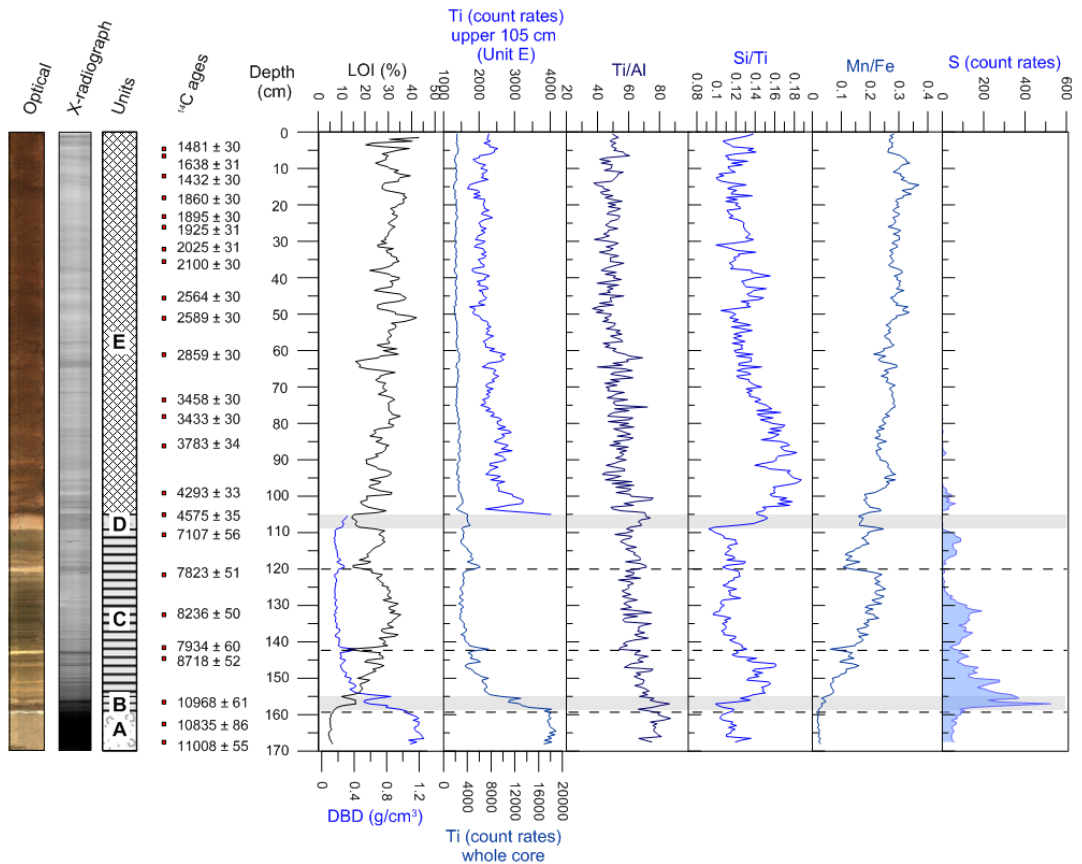


Figure 2: Compiled selected sedimentological parameters from AMP-112. Optical line-scan image and radiographic image show the sediment colour and density (darker colours represent denser sediment), respectively. Lithological log shows unit division (also indicated in horizontal light grey bars). All XRF data are smoothed to 0.5 cm resolution. Ti count rates are plotted for both the whole core length, and also zoomed in for the upper 105 cm due to change in count rates in Unit C (note change in scale). Ti count rates co-vary with Ti/Al ratio. Si/Ti is often used as an indicator of biological silica (productivity) (e.g. Balascio et al., 2011; Melles et al., 2012), and also co-varies with Ti/Al. Mn/Fe indicates increasingly oxic conditions (e.g. Naehler et al., 2013) towards the top of the core. Horizons of inferred instantaneously deposited sediments (cf. section 4.2) are highlighted with dashed lines.

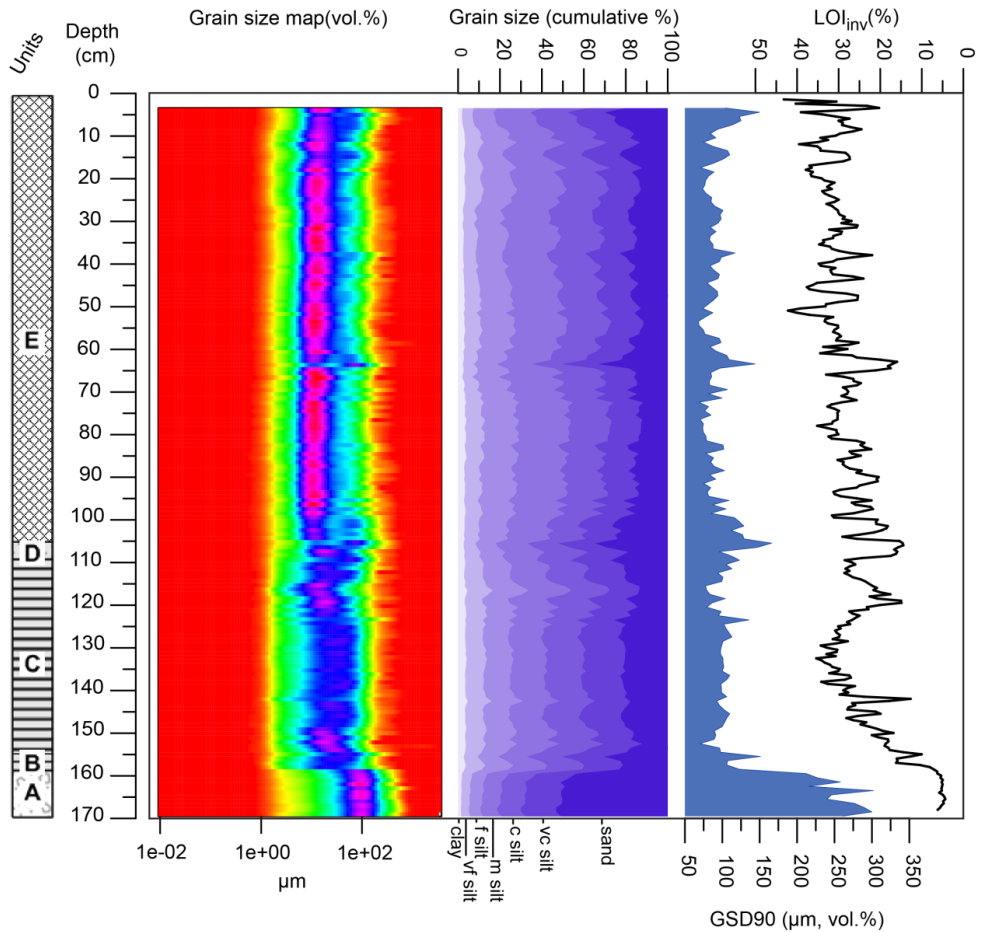


Figure 3: GSD (volume %) plotted as a surface diagram, with darker blue/purple colour where the frequency of particular grain sizes is highest (plotted using software 'EMMAgeo'; Dietze and Dietze, 2013). The well-sorted, fine-grained Unit E is easily visually distinguishable from the coarser-grained units A-D. Cumulative plot highlights the background sediment with silt making up most of the sediment. 90 percentile GSD reveals that the volume of Unit A contains coarser-grained particles, and the more similar variance in grain sizes throughout units B-E. LOI (%) is plotted on inverted scale, reflecting varying organic content throughout the core, co-varying inversely with GSD90 ($R=-0.5$). Note rapid drops in organic content during intervals of larger GSD.

4.3 Environmental evolution of Hakluytvatnet- inferences from diatom analyses

The main findings from the diatom analyses are presented in Fig. 4, and placed in environmental context below.

Two significantly different environments are identified from the diatom analysis: an early unstable, silt- and clay-dominated environment (units A-C), and a later, more productive clear water lake environment (units D-E). Initially, in samples from Unit A (160.5 cm), the diatom flora is characterized by the presence of species of *Muelleria*, *Diadesmis*, *Luticola* which are associated with polar subaerial environments, including cryoconite, soils, and microbial mats (cf. Johansen, 2010; van de Vijver et al., 2014). *Pinnularia* spp. and *Stauroneis gracilis* complex = cf. *S. gracilis*, *S. pax*, *S. vandevijveri*) are also present, the latter of which have been found in very shallow pools/seepages in elsewhere in the high Arctic (van de Vijver et al., 2004). Together, these suggest that Hakluytvatnet was not yet a lake, but a terrestrial landscape with a nascent soil and biofilm microbial community. This unit transitions to Unit B (sampled at 158 cm), where the soil diatoms have largely disappeared, and are replaced by *Navicula digitulus*, as well as small pioneering *Fragilaria s.l.* species (*Staurosirella pinnata*, *Pseudostaurosira pseudoconstruens*), a community characteristic of cold, oligotrophic, postglacial lake environments with high sedimentation rates (cf. Perren et al., 2012; Wojtal et al., 2014). In two samples from Unit C (150 and 130 cm), small fragilarioids continue to dominate (*S. pinnata*, *P. pseudoconstruens*, *S. exiguiformis*) as well as very small *Navicula*. cf. *submuralis*, suggesting a typically nutrient-poor, high-arctic lake, where suspended sediment load still precludes the development of a planktonic diatom community. Samples from units D (108 cm) and E (98 cm) record a fundamental shift to a more productive lake environment that supports a higher diversity of benthic as well as planktonic taxa (e.g. *Aulacoseira distans*). In these last units, most of the clay is gone, improving the light quality, and allowing for colonization and enhanced biological activity in all parts of the lake. This is

in agreement with the observed increase in Si/Ti at the transition to Unit E, which also suggests an increased production of biogenic silica (Fig 2).

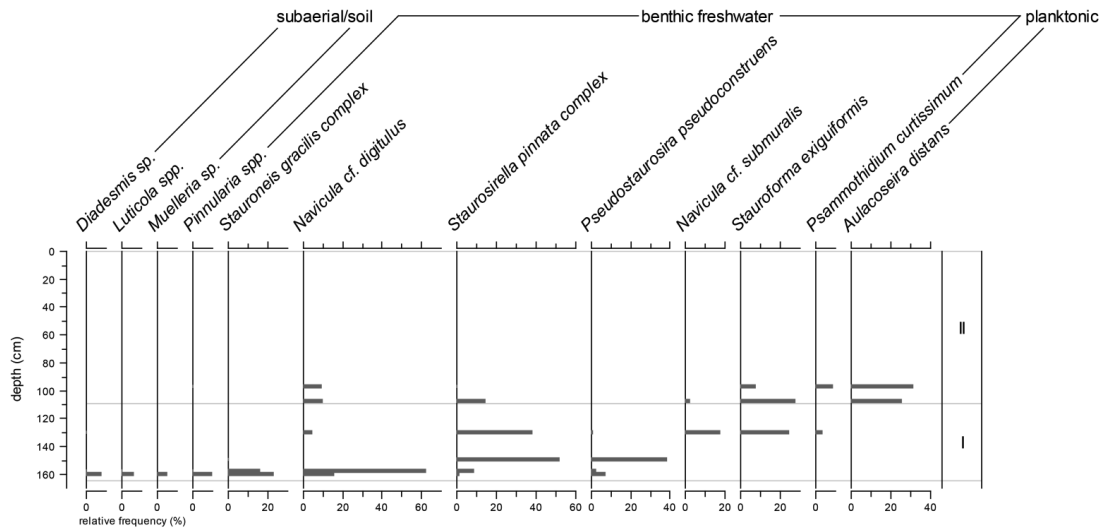


Figure 4: Percent abundance of diatom taxa that indicate environmental evolution of the lake and landscape. The two significant zones in the core stratigraphy are highlighted.

4.4 Principal component analysis

Ordination with PCA returned one significant Principal Component (PC) axis; explaining 49% of the variability in the dataset from the upper 105 cm of AMP-112. Most of the geochemical elements, except Sr and Mg, align closely with PCA1, with Mn correlating positively with LOI and the remaining elements correlating inversely with LOI (Si, K, Ca, Ti, and Fe). The second PC axis captures mainly the variability of GSD90 and Mg, although this axis may not be significant, explaining only 11% of the total variability. This shows that variations in grain size are not correlated with general changes in geochemistry, although there is a weak inverse correlation with Mg. Visually it is apparent that large GSD perturbations often occur at the same time as large fluctuations in the XRF data, but there is

no clear relationship in the direction of change, and additionally there is a long-term trend in the geochemical elements that is not observed in GSD. A linear detrending of the dataset increases the correlation between GSD90 and LOI, whereas it decreases the correlation between LOI and the geochemical elements. This could indicate that the long-term trend in the XRF-data is driven by LOI and water content through dilution of the XRF signal, which means that geochemistry and LOI are not governed by the same process(es) on shorter timescales. After detrending, the strongest correlation is found between GSD90 and LOI ($R=0.50$), suggesting some common driver of these signals.

4.5 Chronology and sedimentation rates

Compaction during piston coring caused loss of the sediment-water interface in core AMP-112, and pressed the upper soft sediments together. Intra-basin correlation between the short cores (AMD-0212 and AMD-0112) and AMP-112 was done based on XRF Ti count rates in order to construct a common depth scale for the cores and produce a composite age-depth model. In Fig. 5A the radiocarbon-based AMP-112 age-depth model produced in ‘Bacon’ is stippled with the 95% uncertainty range derived from the radiocarbon ages highlighted in grey. Also plotted in Fig. 5A is the PSV-synchronized age-depth relationship constructed from radiocarbon dates from both Hakluytvatnet and Lake Hajeren along with several PSV-synchronized tie points between the lakes. The individual control points are colour-coded for each source of origin (Fig. 5A).

Sediment accumulation rate (SAR) at Hakluytvatnet (Fig. 5B) changed significantly throughout the core. Periods of non-deposition, or extremely low SAR, <0.01 (cm/yr), are found at two intervals; $\sim 12,700 - \sim 9700$ cal yr BP and from $\sim 8400 - \sim 5300$ cal yr BP. Between these two periods, a significant increase in SAR (up to ~ 0.05 cm/yr) is seen around

9500 cal yr BP. After 5300 cal yr BP, the SAR gradually increases and varies more frequently and with larger amplitudes than in the lower sediment sequence. Several short-lived spikes in SAR are found centred at ~4800, ~3800, ~2900, ~1900 and ~350 cal yr BP (Fig. 5B).

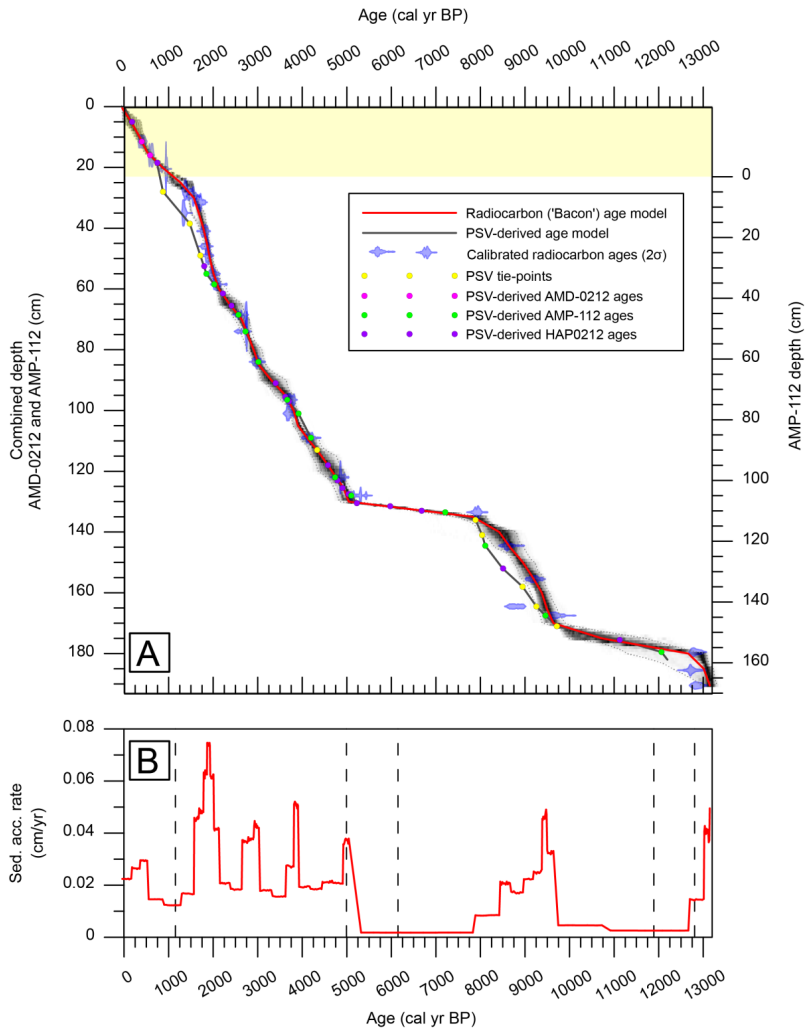


Figure 5: A) Age-depth relationship for AMP-112 and AMD-0112. Radiocarbon (‘Bacon’) age-model in grey shaded area (95% confidence interval); transparent blue points denote individual calibrated ^{14}C ages. ‘Best’ age-depth relationship (red solid line) is based on the weighted mean age for each depth. The PSV-corrected age-depth model is marked as a dark grey line including colour-coded PSV-derived radiocarbon ages from AMP-112 and AMD-0212, PSV tie-points (Ólafsdóttir et al., 2016), and radiocarbon ages from HAP0212 (van der Bilt et al., 2015). PSV-derived age model is truncated at transition to Unit A (159 cm depth AMP-112 depth scale; c.f. sections 4.5/5.2). Depth scales are shown both as the combined

depth scale coupling AMD-0212 and AMP-112 (left) and as individual AMP-112 depth scale (right) (+23 cm [yellow shaded area] added to AMD-0212; c.f. section 4.5. B) Sediment accumulation rate calculated from 'Bacon'-derived age-depth relationship. Dashed lines denote lithological unit divisions of AMP-112 (core top age: ~1150 cal yr BP).

4.6 Equilibrium-line altitude reconstruction

Modern-day regional equilibrium-line altitude (ELA) is situated above the highest point of the catchment area, i.e. above ~400 m a.s.l. (regional ELA overview in: Hagen et al., 2003). We estimated the ELA of the glacier that deposited the moraine ridge NW of the lake (Fig. 1C) based on a simple cartographic reconstruction of the palaeo-glacier's hypsometry. Calculating palaeo-ELAs can be done in several ways, but due to the few constraints available to define the glacier geometry (e.g. lateral moraines), we have chosen to apply the Accumulation Area Ratio (AAR) and the Area-Altitude Balance Ratio (AABR) methods (e.g. Benn and Lehmkuhl, 2000; Osmaston, 2005).

The AAR method assumes that the accumulation area constitutes a fixed ratio of the total glacier area, and the ratio applied for cirque and valley glaciers (as here) is normally ~0.6 (Benn and Evans, 1998; Rea, 2009), whereas the AABR method takes into account both glacier hypsometry and the difference between the accumulation and ablation gradients (Rea, 2009). We calculated ELAs for the palaeo-glacier using a range of AAR values between 0.65 and 0.45, which returned ELAs ranging from 50-180 m a.s.l.; with a mean of 60 and 125 m a.s.l. for AAR of 0.6 ± 0.5 and 0.5 ± 0.5 , respectively (Table 2). As such, we find that the hypsometry of the palaeo-glacier, which includes a steep and narrow part between 150 and 250 m a.s.l., makes it very sensitive to small changes in accumulation area within the likely AAR range investigated here. The AABR ratios applied are calculated from the regional Svalbard range (2.13 ± 0.52) from the compilation in Rea (2009) and are also presented in Table 2. The palaeo-ELAs calculated applying the AABR method display a narrower range

from 150-175 m a.s.l., which is within the wider AAR range. With the limited data available, we conclude that the ELA of the Hakluyvatnet palaeo-glacier was situated somewhere between 50 – 180 m a.s.l. when the moraine ridge north of Hakluyvatnet was deposited. Although there are large uncertainties in our ELA estimate, it highlights that the regional ELA does not have to be lowered very much to allow glaciation in the catchment, i.e. in the range of 100-200 m (Hagen et al., 2003).

Table 2: ELA's calculated for the reconstructed palaeo-glacier covering Hakluyvatnet.

Ratio	AAR ELA (m a.s.l.)		Balance ratio ELA (m a.s.l.)	
	0.45	0.65	1.61	2.65
Palaeo-glacier Hakluyvatnet	180	50	150	175

DISCUSSION

The main objective of this study has been to reconstruct the Late Glacial and Holocene climate history of Amsterdamøya based on sediments deposited in lake Hakluyvatnet. Below we discuss the deglaciation history, the large environmental changes observed in the Early- and Mid-Holocene, and finally, late Holocene changes in hydroclimate, based on interpretations of the lake record.

5.1 Chronology

The results from PSV-synchronizing between the lakes Hakluytvatnet and Hajeren highlight the potential of applying this methodology on high-Arctic lakes where robust radiocarbon chronologies are usually challenging to construct due to a general lack of organic detritus. However, due to two intervals in the core showing relatively large offsets in age between the two age-modelling approaches, as well as the large number of radiocarbon ages obtained for the Hakluytvatnet lake record ($n=28$), we have chosen to simply use the ‘Bacon’-derived age-depth relationship for plotting our lake proxies against age.

5.2 Late Glacial ELA reconstruction

The massive diamicton constituting Unit A in core AMP-112 from Hakluytvatnet is interpreted as a basal till deposited just prior to the final deglaciation of the Hakluytvatnet catchment. Two radiocarbon dates within the till, and one directly overlying it, returned overlapping ages (see Table 1) centred around 12,800 cal yr BP. From the geomorphological mapping our interpretation is that the moraine ridge deposited outside Hakluytvatnet (Fig. 1C) was formed by a local cirque glacier occupying the catchment covering the lake, and the basal till in AMP-112 is therefore interpreted to be related to this local glacier re-advance and not the Barents Sea Ice Sheet (BSIS). During the Last Glacial Maximum (LGM) ice extended to the shelf break some 8 km northwest of Amsterdamøya (Ingólfsson and Landvik, 2013), leaving most of the Hakluytvatnet catchment covered by a glacier, although the highest areas of Amsterdamøya were probably ice-free (Landvik et al., 2003). The Hakluytvatnet catchment might therefore have become more-or-less ice-free when the BSIS first retreated from the northwest Spitsbergen area around ~13,800 cal yr BP (~12 ^{14}C ka BP) (Ingólfsson and Landvik, 2013), and from our interpretation a local cirque glacier then formed and advanced

across Hakluytvatnet, before finally retreating in the early Younger Dryas (~12,800 cal yr BP). This could imply that this glacier advance commenced sometime during the warmer Bølling-Allerød period, and that it was initiated by increased precipitation and favourable wind conditions in the form of prevailing polar easterlies (Birgel and Hass, 2004). During the transition to the colder YD, moisture starvation induced by increased sea-ice cover (e.g. Müller et al., 2009) likely caused the demise of the cirque glacier, and the Hakluytvatnet lake has not been covered by a glacier ever since. OSL and radiocarbon ages centred around 50 ka of the sediment ('valley-fill') below the moraine ridge (Landvik et al., 2003) indicate that the stratigraphically younger moraine was deposited sometime after 50 ka. Thus, we acknowledge that the moraine ridge might be older than the glacier event detected in the sediment core, but our interpretation that Unit A is a subglacially deposited diamict implies that the glacier at least covered the part of the lake where the core was retrieved and the ridge acts as a maximum estimate of the palaeo-glacier extent. As there are no indications of marine sedimentation in Hakluytvatnet, sea level must have remained at below the top part of this ridge at 16 m a.s.l. ever since deglaciation and it is therefore not necessary to adjust our estimated palaeo-ELA due to changes in relative sea level. Relative to the highest point of the present-day snowfield (~400 m a.s.l.; Fig. 1C), the reconstructed ELA lowering is on the order of ~220 – 350 m (AAR) and from 225 – 250 m (AABR) (Table 2). This is comparable with YD ELA lowering in Northern Norway of ~370 m (Rea and Evans, 2007) and a recent study from Northern Norway showing 220 and 130 m ELA lowering during the Late Glacial and the YD, respectively (Wittmeier et al., submitted).

Our ELA estimate is the first YD ELA estimate from NW Svalbard, whereas in western Svalbard glacier extent has generally been thought to be larger during the LIA than during YD (Mangerud and Landvik, 2007). This may reflect that the west coast glaciers were located in the precipitation shadow from possible prevailing YD easterlies (Birgel and Hass, 2004),

thereby reducing accumulation on these glaciers. The Hakluytvatnet catchment receives snowdrift from the plateau, though mostly from snow that accumulates from N-NE winds, which could further support the idea that YD atmospheric conditions (e.g. Mayewski et al., 1993) could support a glacier in the Hakluytvatnet catchment for a short while before it started retreating.

5.3 Early and Mid-Holocene depositional environment

During the early- and mid-Holocene, the depositional environment changed significantly for Hakluytvatnet, which can be easily seen from the lithostratigraphy of AMP-112. Large shifts in the environment are reflected in changing SAR and geochemical properties, as well as environmental shifts detected in diatom assemblages when the lake was transitioning from a dry polar soil/biofilm environment to an oligotrophic lake (section 4.3).

During deposition of Unit B (~12,800 – ~11,900 cal yr BP), the diatom assemblage indicates that the sedimentary environment was likely a cold postglacial lake environment (cf. section 4.3), and this is further supported by low Si/Ti values (Fig. 2), which reflect low production of biogenic silica (e.g. Balascio et al., 2011; Melles et al., 2012). Unit C represents the early-Holocene depositional environment in lake Hakluytvatnet (~11,900 – ~6150 cal yr BP), and is clearly distinguishable from Units A and B below. The diatom assemblage is typical of a nutrient-poor, high-Arctic lake where not much is living in the photic zone. Unit C is suggested to reflect an anoxic depositional environment (as indicated by high sulphur counts and low Mn/Fe ratios; Fig. 2) and this might, combined with the nutrient-poor environment indicated by the diatom analyses, suggest that the lake was covered by lake ice for a longer period of the year than what is presently the case. Freshwater forcing by meltwater pulses originating from the decaying ice sheets in the North Atlantic induced enhanced seasonality

and unstable climatic conditions during the Early Holocene (e.g. Beck et al., 1997; Stager and Mayewski, 1997; Renssen et al., 2002), and we suggest that the more extreme seasonality during the Early Holocene (e.g. Haug et al., 2001) could have acted as a driver for stratification of the lake during the HTM, with more severe winters inducing a longer ice cover season. Additionally, shallowing lake levels could have progressed until the aquatic mosses were able to establish on the bed of the succeeding clearer lake waters (~5000 cal yr BP), in conjunction with turnover by wind on the smaller surface area of the lake preventing any strong stratification ever since.

Unit D (~6150 – ~5000 cal yr BP) either represents a period of very low sedimentation rate, or a hiatus in deposition when the lake might even have disappeared completely as a result of the warmer and drier climate of the Mid-Holocene on Svalbard, as is recorded in terrestrial (Birks, 1991) and marine records (Salvigsen, 2002). We can only speculate as to why the lake dried out, but conclude that there was a large shift in depositional environment at the time of Unit D being deposited, which is also reflected in the diatom assemblages with a shift to a more diverse lake environment and improved light quality. Increased productivity is also reflected in the large increase in Si/Ti (Fig. 2). At this point we make no conclusions about what caused this transition, and we have chosen to focus mainly on the last ~5000 years for the remainder of this discussion, because it reflects a stable depositional environment in Hakluytvatnet, and because this period is particularly interesting with respect to the Neoglacial period on Svalbard (e.g. Røthe et al., 2015). Furthermore, our age-model is well constrained for this time period.

5.4 Neoglacial runoff and productivity changes in Hakluytvatnet

The late-Holocene part of the sediment record from AMP-112 represented by Unit E covers the time period from ~5000 cal yr BP to ~1100 cal yr BP. Based on our geomorphological mapping and understanding of active earth surface processes in the catchment, we interpret changes in detrital input to Hakluytvatnet during the last 5000 cal yr BP (i.e. the Neoglacial) as primarily reflecting precipitation- or meltwater-induced sediment transport from the surrounding catchment area, as the flat topography surrounding the lake does not promote mass-wasting processes. Changes in grain size (GSD90) might therefore reflect changes in the intensity of precipitation events. The fairly strong (negative) correlation ($R=-0.5$) between GSD90 and detrended LOI suggests that periods of more intense precipitation and runoff is also an important driver for increased minerogenic sedimentation in the lake. Based on the GSD90 record, increased runoff intensity at Hakluytvatnet is observed during four distinct intervals: between ~1600 – ~1350 (top of runoff record) cal yr BP; between ~2250 – ~2150 cal yr BP; between ~3150 – ~3000 cal yr BP; and between ~5000 – ~4800 cal yr BP (grey vertical bars in Fig. 6).

The diatom analysis provides snapshots of detailed environmental information for Hakluytvatnet (Fig. 4), and it shows a distinct change to a more productive clear-water environment around 5000 cal yr BP. At the same level we observe a strong increase in the XRF Si/Ti ratio, which in some cases can act as a proxy for biogenic silica (e.g. Balascio et al., 2011; Melles et al., 2012), and thereby reflect internal productivity in the lake. This is based on the argument that Ti can only be provided to the lake sediments through detrital input while Si can be provided both through detrital input and through diatom growth in the lake. Seeing that the sharp increase in Si/Ti around 5000 cal yr BP coincides with a change in diatom flora that reflects increased productivity, we suggest that the Si/Ti ratio does reflect production of biogenic silica in Hakluytvatnet, thereby providing a high-resolution record of

productivity change for the entire Neoglacial period on Svalbard. The highest productivity is indicated between 5000-4000 cal yr BP, after which a gradual decrease is seen (Fig. 6). This pattern follows the general trend of decreasing insolation at high northern latitudes; however, the maritime setting of Hakluytvatnet should also make this site highly sensitive to oceanic influence. When initiation of modern oceanographic conditions in the eastern Fram Strait occurred ~5200 cal yr BP (Werner et al., 2013) this allowed for the WSC to transport heat and moisture up to NW Svalbard. This adjustment in oceanic configuration could explain the change in boundary conditions in the Hakluytvatnet catchment around the same time. During the Neoglacial, the decreasing trend in summer insolation (Huybers, 2006) (Fig. 6C) is also reflected in increasing sea ice extent (Müller et al., 2012) (Fig. 6C). Productivity in Hakluytvatnet (Fig. 6B and C) displays similar trends as changes in sea-ice extent in the Fram Strait, indicating that the distribution of sea ice greatly impacts lake productivity. Reduced sea ice thereby seems to promote lake productivity, reflecting milder and wetter (i.e. more maritime) conditions. The Si/Ti record from Hakluytvatnet could therefore provide a high-resolution record of local sea ice conditions around Amsterdamøya. As sea ice cover is a key factor in controlling the moisture availability for Svalbard, particularly for the very northernmost coast where Hakluytvatnet is situated, it should also impact runoff from the Hakluytvatnet catchment. Looking at the GSD90 record, we observe that there seems to be an increase in runoff-induced sedimentation to Hakluytvatnet during periods of decreasing sea ice extent, as reflected in higher Si/Ti values (Fig. 6C). We therefore suggest that the runoff record reflects the atmospheric moisture supply to the Hakluytvatnet catchment, which is highly dependent on the prevailing sea-ice conditions. There might also be a component related to atmospheric circulation in the runoff record, reflecting changes in for instance the Arctic Oscillation (AO). In instrumental data, a link is seen between increased snow-depth in SW Svalbard and a more negative AO index (Luks et al., 2011), making it possible that this

large-scale circulation feature might affect runoff to Hakluytvatnet. Though, variability in sea level pressure caused by AO changes might affect sea ice configuration that in turn affect moisture supply to the Hakluytvatnet catchment. However, as our runoff record does not overlap with instrumental data, we cannot establish a firm connection between atmospheric circulation and our lake data.

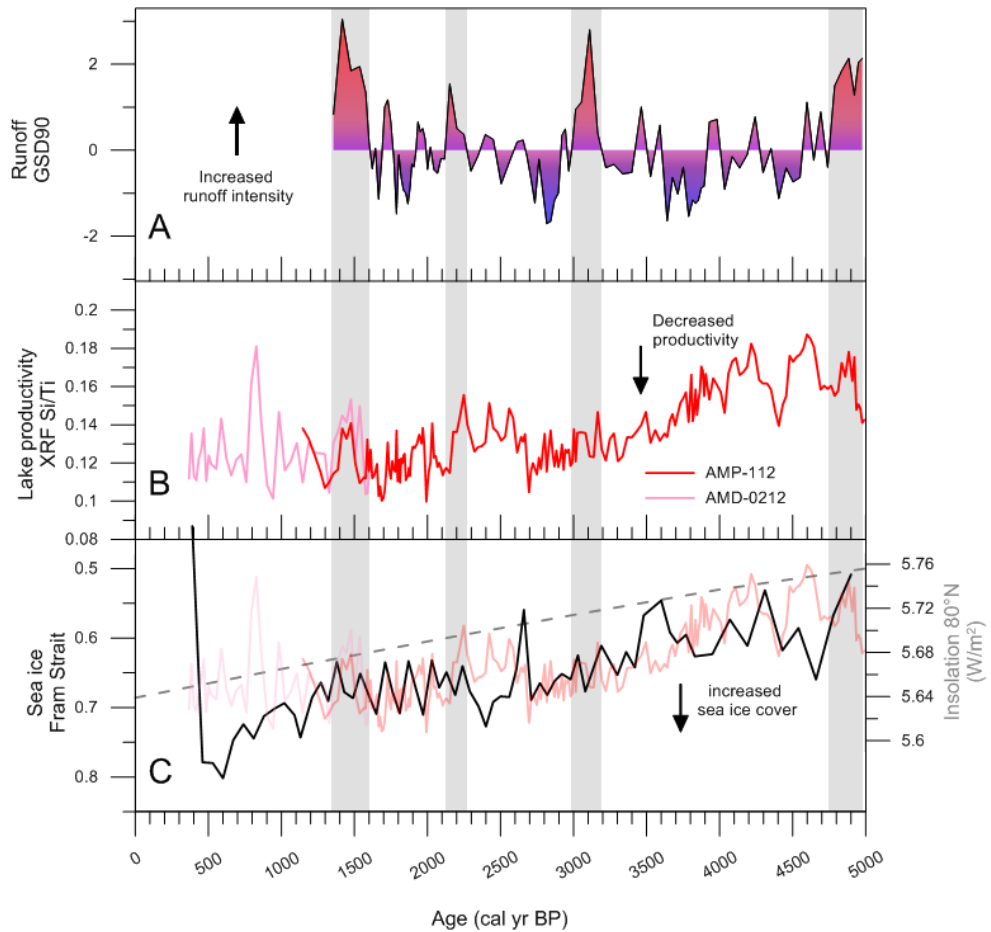


Figure 6: A) Runoff record from Hakluytvatnet (standardized and detrended GSD90); B) lake productivity record (XRF Si/Ti ratios, coupling AMP-0212 and AMP-112 [cf. section 4.5 and Fig. 5]); C) total solar insolation (dashed line) at 80°N (Huybers, 2006) and reconstructed sea ice variability in the Fram Strait from sea ice biomarker proxy IP_{25} (sediment core MSM5/5-712-2) (Müller et al., 2012). Also plotted in C) are Si/Ti XRF ratios as in B) to highlight covariance. Grey vertical bars denote periods with relatively large runoff.

CONCLUSIONS

- Fundamental changes in the depositional environment represented by the sediments reveal large changes in the hydrology of northwest Svalbard during the Holocene and the Hakluytvatnet record gives insight into these large changes
- We present the first (terrestrial?) evidence for a larger YD glacier extent on Svalbard than during the LIA and propose that the glacier extent was governed by favourable winds and precipitation before subsequent YD cooling and sea-ice expansion led to glacier starvation. The glacier retreated rapidly up-valley 12,800 cal yr BP
- Between 12,800 – 11,900 cal yr BP dry conditions precluded the formation of a lake or cold conditions led to a shallow lake that was frozen to the bottom. Sediment accumulated very slowly
- Between 11,900 – 6150 cal yr BP increased moisture led to a lake in the basin. In-wash of silt from the catchment made it a murky lake and restricted the growth of aquatic mosses
- Between 6150 – 5000 cal yr BP the lake completely dried up at this time and no sediment was deposited, likely as a result of the warm Holocene Thermal Optimum
- The onset of Neoglacial conditions ~5000 cal yr BP resulted in a positive moisture balance for the site and allowed the lake to form. Clear water allowed aquatic moss to grow. Punctuated episodes of clastic in-wash point toward rapid snowmelt events or high summer precipitation events that carried minerogenic material into the lake
- The sedimentary signal in the lake since ~5000 cal yr BP reflects extreme runoff from the catchment, and we constructed a time-series of runoff at NW Svalbard
- Further, we have constructed a time-series reflecting productivity that seems highly influenced by sea ice variability, thereby showing the potential of applying

productivity changes in Hakluytvatnet as a high-resolution proxy for sea ice variability at the northwesternmost corner of Svalbard

ACKNOWLEDGEMENTS

Permission to perform field work in the national park during both expeditions was granted by the Governor of Svalbard (RIS ID 5155, ref.: 2012/00753-11 a.512). We thank Bjørn C. Kvisvik, Rob D'Anjou and Greg de Wet for assistance during field work, and acknowledge funding by Svalbard Science Forum (AFG project no. 235919) as well as funding from the Norwegian Research Council via the SHIFTS project. Atle Nesje is thanked for giving constructive comments on the manuscript, and Gunhild Rosqvist is thanked for commenting an earlier draft of the manuscript. Eivind Støren is thanked for technical assistance with settings of the Mastersizer. Anne Bjune helped identify multiple macrofossil samples. PSV scan supervised by Joseph Stoner, Oregon State University. Micha Dietze is thanked for help with coding in EMMAgeo software. Radiocarbon dating was conducted in: Uppsala, Sweden (supervised by Göran Possnert and Elisabet Petterson); Poznan, Poland (supervised by Thomas Goslar), ETH, Switzerland, Direct AMS, USA (supervised by Ugo Zoppi).

REFERENCES

- Aagaard, K., Foldvik, A., Hillman, S., 1987. The West Spitsbergen Current: disposition and water mass transformation. *Journal of Geophysical Research: Oceans* (1978–2012) 92, 3778-3784
- ACIA, 2004. *Impacts of a Warming Arctic: Arctic Climate Impact Assessment, Impacts of a Warming Arctic*, Cambridge, UK, p. pp. 144.
- Antoniades, D., Hamilton, P., Douglas, M.S.V., Smol, J.P., 2008. Freshwater diatoms of the Canadian High Arctic Islands: Ellef Ringnes, northern Ellesmere and Prince Patrick islands, *Iconographia Diatomologica*. A.R.G. Gantner Verlag, Ruggell, p. 649.
- Bakke, J., Trachsel, M., Kvisvik, B.C., Nesje, A., Lyså, A., 2013. Numerical analyses of a multi-proxy data set from a distal glacier-fed lake, Sørsendalsvatn, western Norway. *Quaternary Science Reviews* 73, 182-195
- Balascio, N.L., Zhang, Z., Bradley, R.S., Perren, B., Dahl, S.O., Bakke, J., 2011. A multi-proxy approach to assessing isolation basin stratigraphy from the Lofoten Islands, Norway. *Quaternary Research* 75, 288-300
- Beck, J.W., Récy, J., Taylor, F., Edwards, R.L., Cabioch, G., 1997. Abrupt changes in early Holocene tropical sea surface temperature derived from coral records. *Nature* 385, 705-707
- Benn, D.I., Evans, D.J., 1998. *Glaciers and glaciation*, London.
- Benn, D.I., Lehmkuhl, F., 2000. Mass balance and equilibrium-line altitudes of glaciers in high-mountain environments. *Quaternary International* 65, 15-29
- Birgel, D., Hass, H.C., 2004. Oceanic and atmospheric variations during the last deglaciation in the Fram Strait (Arctic Ocean): a coupled high-resolution organic-geochemical and sedimentological study. *Quaternary Science Reviews* 23, 29-47
- Birks, H.H., 1991. Holocene vegetational history and climatic change in west Spitsbergen-plant macrofossils from Skardtjørna, an Arctic lake. *The Holocene* 1, 209-218
- Birks, H.J.B., Monteith, D.T., Rose, N.L., Jones, V.J., Peglar, S.M., 2004. Recent environmental change and atmospheric contamination on Svalbard as recorded in lake sediments—modern limnology, vegetation, and pollen deposition. *Journal of Paleolimnology* 31, 411-431
- Blaauw, M., Christen, J.A., 2011. Flexible paleoclimate age-depth models using an autoregressive gamma process. *Bayesian Analysis* 6, 457-474
- Boulton, G.S., Rhodes, M., 1974. Isostatic uplift and glacial history in northern Spitsbergen. *Geological Magazine* 111, 481-500.[doi:10.1017/S0016756800041546](https://doi.org/10.1017/S0016756800041546)

- Croudace, I.W., Rindby, A., Rothwell, R.G., 2006. ITRAX: description and evaluation of a new multi-function X-ray core scanner. *Special Publication - Geological Society Of London* 267, 51
- Dean, W.E., 1974. Determination of carbonate and organic matter in calcareous sediments and sedimentary rocks by loss on ignition: comparison with other methods. *Journal of Sedimentary Research* 44
- Dietze, M., Dietze, E., 2013. EMMAgeo: End-member modelling algorithm and supporting functions for grain-size analysis, R package version 0.9. 0.
- Førland, E.J., Benestad, R., Flatøy, F., Hanssen-Bauer, I., Haugen, J., Isaksen, K., Sorteberg, A., Ådlandsvik, B., 2009. Climate development in North Norway and the Svalbard region during 1900–2100.
- Førland, E.J., Benestad, R.E., Flatøy, F., Hanssen-Bauer, I., Haugen, J.E., Isaksen, K., Sorteberg, A., Ådlandsvik, B., 2010. Klimautvikling i Nord-Norge og på Svalbard i perioden 1900–2100: klimaendringer i norsk Arktis: NorACIA delutredning 1.
- Hagen, J.O., Melvold, K., Pinglot, F., Dowdeswell, J.A., 2003. On the net mass balance of the glaciers and ice caps in Svalbard, Norwegian Arctic. *Arctic, Antarctic, and Alpine Research* 35, 264-270
- Haug, G.H., Hughen, K.A., Sigman, D.M., Peterson, L.C., Röhl, U., 2001. Southward migration of the intertropical convergence zone through the Holocene. *Science* 293, 1304-1308
- Heiri, O., Lotter, A.F., Lemcke, G., 2001. Loss on ignition as a method for estimating organic and carbonate content in sediments: reproducibility and comparability of results. *Journal of Paleolimnology* 25, 101-110
- Hjelle, A., Ohta, Y., 1974. Contribution to the geology of north western Spitsbergen, In: SKRIFTER, N.P. (Ed.), Nr 158, pp. 1-107.
- Hormes, A., Gjermundsen, E.F., Rasmussen, T.L., 2013. From mountain top to the deep sea—deglaciation in 4D of the northwestern Barents Sea ice sheet. *Quaternary Science Reviews* 75, 78-99
- Huybers, P., 2006. Early Pleistocene glacial cycles and the integrated summer insolation forcing. *Science* 313, 508-511
- Ingólfsson, Ó., Landvik, J.Y., 2013. The Svalbard–Barents Sea ice-sheet—Historical, current and future perspectives. *Quaternary Science Reviews* 64, 33-60

- Johansen, J.R., 2010. Diatoms of aerial habitats, In: Smol, J.P., Stoermer, E.F. (Ed.), *The diatoms: applications for the environmental and earth sciences*. Cambridge University Press, Cambridge, UK, pp. 287-308.
- Jørgensen, C.J., Johansen, K.M.L., Westergaard-Nielsen, A., Elberling, B., 2015. Net regional methane sink in High Arctic soils of northeast Greenland. *Nature Geoscience* 8, 20-23
- Kattsov, V.M., Walsh, J.E., Chapman, W.L., Govorkova, V.A., Pavlova, T.V., Zhang, X., 2007. Simulation and projection of Arctic freshwater budget components by the IPCC AR4 global climate models. *Journal of Hydrometeorology* 8, 571-589
- Landvik, J.Y., Bondevik, S., Elverhøi, A., Fjeldskaar, W., Mangerud, J., Salvigsen, O., Siegert, M.J., Svendsen, J.-I., Vorren, T.O., 1998. The last glacial maximum of Svalbard and the Barents Sea area: ice sheet extent and configuration. *Quaternary Science Reviews* 17, 43-75
- Landvik, J.Y., Brook, E.J., Gualtieri, L., Raisbeck, G., Salvigsen, O., Yiou, F., 2003. Northwest Svalbard during the last glaciation: Ice-free areas existed. *Geology* 31, 905-908
- Lepš, J., Šmilauer, P., 2003. *Multivariate Analysis of Ecological Data using CANOCO*. Cambridge University Press, Cambridge.
- Luks, B., Osuch, M., Romanowicz, R.J., 2011. The relationship between snowpack dynamics and NAO/AO indices in SW Spitsbergen. *Physics and Chemistry of the Earth, Parts A/B/C* 36, 646-654
- Löwemark, L., Chen, H.-F., Yang, T.-N., Kylander, M., Yu, E.-F., Hsu, Y.-W., Lee, T.-Q., Song, S.-R., Jarvis, S., 2011. Normalizing XRF-scanner data: a cautionary note on the interpretation of high-resolution records from organic-rich lakes. *Journal of Asian Earth Sciences* 40, 1250-1256
- Mangerud, J., Dokken, T., Hebbeln, D., Heggen, B., Ingólfsson, Ó., Landvik, J.Y., Mejdahl, V., Svendsen, J.I., Vorren, T.O., 1998. Fluctuations of the Svalbard–Barents Sea Ice Sheet during the last 150 000 years. *Quaternary Science Reviews* 17, 11-42
- Mangerud, J., Landvik, J.Y., 2007. Younger Dryas cirque glaciers in western Spitsbergen: smaller than during the Little Ice Age. *Boreas* 36, 278-285
- Mayewski, P.A., Meeker, L.D., Whitlow, S., Twickler, M.S., Morrison, M.C., Alley, R.B., Bloomfield, P., Taylor, K., 1993. The atmosphere during the Younger Dryas. *Science* 261, 195-197
- Melles, M., Brigham-Grette, J., Minyuk, P.S., Nowaczyk, N.R., Wennrich, V., DeConto, R.M., Anderson, P.M., Andreev, A.A., Coletti, A., Cook, T.L., 2012. 2.8 million years of Arctic climate change from Lake El'gygytyn, NE Russia. *Science* 337, 315-320

- Merrill, R.T., McElhinny, M., McFadden, P.L., 1996. The magnetic field of the earth: paleomagnetism, the core, and the deep mantle. Academic Press, San Diego, CA.
- Müller, J., Massé, G., Stein, R., Belt, S.T., 2009. Variability of sea-ice conditions in the Fram Strait over the past 30,000 years. *Nature Geoscience* 2, 772-776
- Müller, J., Werner, K., Stein, R., Fahl, K., Moros, M., Jansen, E., 2012. Holocene cooling culminates in sea ice oscillations in Fram Strait. *Quaternary Science Reviews* 47, 1-14
- Naeher, S., Gilli, A., North, R.P., Hamann, Y., Schubert, C.J., 2013. Tracing bottom water oxygenation with sedimentary Mn/Fe ratios in Lake Zurich, Switzerland. *Chemical Geology* 352, 125-133
- Ohta, Y., Hjelle, A., Dallmann, W.K., 2007. Geological map Svalbard 1:100 000, sheet A4G, Vasahalvøya., Temakart nr. 40. ed. Norsk Polarinstitutt
- Osmaston, H., 2005. Estimates of glacier equilibrium line altitudes by the Area× Altitude, the Area× Altitude Balance Ratio and the Area× Altitude Balance Index methods and their validation. *Quaternary International* 138, 22-31
- Perren, B.B., Anderson, N.J., Douglas, M.S., Fritz, S.C., 2012. The influence of temperature, moisture, and eolian activity on Holocene lake development in West Greenland. *Journal of Paleolimnology* 48, 223-239
- R Development Core Team, 2012. R: A language and environment for statistical computing. R Foundation for Statistical Computing. R Foundation for Statistical Computing, Vienna, Austria.
- Rea, B.R., 2009. Defining modern day Area-Altitude Balance Ratios (AABRs) and their use in glacier-climate reconstructions. *Quaternary Science Reviews* 28, 237-248. <http://dx.doi.org/10.1016/j.quascirev.2008.10.011>
- Rea, B.R., Evans, D.J., 2007. Quantifying climate and glacier mass balance in north Norway during the Younger Dryas. *Palaeogeography, Palaeoclimatology, Palaeoecology* 246, 307-330
- Reimer, P.J., Bard, E., Bayliss, A., Beck, J.W., Blackwell, P.G., Ramsey, C.B., Buck, C.E., Cheng, H., Edwards, R.L., Friedrich, M., 2013. IntCal13 and Marine13 radiocarbon age calibration curves 0–50,000 years cal BP. *Radiocarbon* 55, 1869-1887
- Renberg, I., 1990. A procedure for preparing large sets of diatom slides from sediment cores. *Journal of Paleolimnology* 4, 87-90
- Renssen, H., Goosse, H., Fichet, T., 2002. Modeling the effect of freshwater pulses on the early Holocene climate: The influence of high-frequency climate variability. *Paleoceanography* 17, 10-11-10-16

- Rubensdotter, L., Rosqvist, G., 2009. Influence of geomorphological setting, fluvial-, glaciofluvial-and mass-movement processes on sedimentation in alpine lakes. *The Holocene* 19, 665-678
- Ryżak, M., Bieganski, A., 2011. Methodological aspects of determining soil particle-size distribution using the laser diffraction method. *Journal of Plant Nutrition and Soil Science* 174, 624-633
- Røthe, T.O., Bakke, J., Vasskog, K., Gjerde, M., D'Andrea, W.J., Bradley, R.S., 2015. Arctic Holocene glacier fluctuations reconstructed from lake sediments at Mitrahalvøya, Spitsbergen. *Quaternary Science Reviews* 109, 111-125
- Salvigsen, O., 1977. Radiocarbon datings and the extension of the Weichselian ice-sheet in Svalbard. *Norsk Polarinstitutt Årbok* 1976, 209-224
- Salvigsen, O., 1979. The last deglaciation of Svalbard. *Boreas* 8, 229-231
- Salvigsen, O., 2002. Radiocarbon-dated *Mytilus edulis* and *Modiolus modiolus* from northern Svalbard: climatic implications. *Norsk Geografisk Tidsskrift-Norwegian Journal of Geography* 56, 56-61
- Shakesby, R.A., Dawson, A.G., Matthews, J.A., 1987. Rock glaciers, protalus ramparts and related phenomena, Rondane, Norway: a continuum of large-scale talus-derived landforms. *Boreas* 16, 305-317
- Sperazza, M., Moore, J.N., Hendrix, M.S., 2004. High-resolution particle size analysis of naturally occurring very fine-grained sediment through laser diffractometry: research methods papers. *Journal of Sedimentary Research* 74, 736-743
- Stager, J., Mayewski, P., 1997. Abrupt early to mid-Holocene climatic transition registered at the equator and the poles. *Science* 276, 1834-1836
- Stoner, J., St-Onge, G., 2007. Magnetic stratigraphy in paleoceanography: reversals, excursions, paleointensity and secular variation. *Proxies in Late Cenozoic Paleoclimatology*. Elsevier, 99-137
- Swett, K., Hambrey, M.J., Johnson, D.B., 1980. Rock glaciers in northern Spitsbergen. *The Journal of Geology*, 475-482
- Thomson, J., Croudace, I., Rothwell, R., 2006. A geochemical application of the ITRAX scanner to a sediment core containing eastern Mediterranean sapropel units. *Geological Society, London, Special Publications* 267, 65-77
- Tjallingii, R., Röhl, U., Kölling, M., Bickert, T., 2007. Influence of the water content on X-ray fluorescence core-scanning measurements in soft marine sediments. *Geochemistry, Geophysics, Geosystems* 8

- van de Vijver, B., Beyens, L., Lange-Bertalot, H., 2004. The genus *Stauroneis* in the Arctic and (Sub-) Antarctic-Regions.
- van de Vijver, B., Zidarova, R., Kopalova, K., 2014. New species in the genus *Muelleria* (Bacillariophyta) from the Maritime Antarctic Region. *Fottea* 14, 77-90
- van der Bilt, W.G., Bakke, J., Vasskog, K., D'Andrea, W.J., Bradley, R.S., Ólafsdóttir, S., 2015. Reconstruction of glacier variability from lake sediments reveals dynamic Holocene climate in Svalbard. *Quaternary Science Reviews* 126, 201-218
- Werner, K., Spielhagen, R.F., Bauch, D., Hass, H.C., Kandiano, E., 2013. Atlantic Water advection versus sea-ice advances in the eastern Fram Strait during the last 9 ka: Multiproxy evidence for a two-phase Holocene. *Paleoceanography* 28, 283-295
- Wittmeier, H.E., Schaefer, J.M., Bakke, J., Rupper, S., Paasche, Ø., Schwartz, R., Finkel, R.C., Interhemispheric mountain glacier fluctuations during the Late Glacial period indicate synchronous summer temperature change, submitted to *Geology*.
- Wojtal, A.Z., Ognjanova-Rumenova, N., Wetzel, C.E., Hinz, F., Piatek, J., Kapetanovic, T., Ector, L., Buczko, K., 2014. Diversity of the genus *Genkalia* (Bacillariophyta) in boreal and mountain lakes-taxonomy, distribution and ecology. *Fottea* 14, 225-239